Nanoscale Electrical Excitation of Surface Plasmon Polaritons with a Nanoantenna Tunneling Junction

Delphine Pommier, Zélie Hufschmitt, Cheng Zhang, Yunhe Lai, Gérald Dujardin, Eric Le Moal, Christophe Sauvan, Jean-Jacques Greffet, Jianfang Wang, Elizabeth Boer-Duchemin

Nanoscale electrical excitation of surface plasmon polaritons with a nanoantenna tunneling junction

Delphine Pommier,[†,§] Zélie Hufschmitt,[†] Cheng Zhang,[‡] Yunhe Lai,[¶] Gérald Dujardin,[†] Eric Le Moal,[†] Christophe Sauvan,[‡] Jean-Jacques Greffet,[‡] Jianfang Wang,[¶] and Elizabeth Boer-Duchemin[*,†]

†*Institut des Sciences Moléculaires d'Orsay (ISMO), CNRS, Université Paris-Saclay, Orsay (France)*

‡*Laboratoire Charles Fabry, Institut d'Optique Graduate School, CNRS, Université Paris-Saclay, Palaiseau (France)*

¶*Department of Physics, The Chinese University of Hong Kong, Shatin, Hong Kong SAR, (China)*

§*Present address: Thales Research and Technology, Palaiseau (France)*

E-mail: Elizabeth.Boer-Duchemin@universite-paris-saclay.fr

Abstract

Quantum tunneling-driven optical nanoantennas are key components for the development of integrated plasmonic nanodevices. In this work, we use the tunneling junction between a nanoantenna and a thin gold film to electrically excite propagating surface plasmons on the nanoscale. The nanoantenna is a chemically synthesized gold nanocube ($\sim$ 50-nm side length) that is separated from a thin (50-nm) gold film by an

insulating molecular layer (1,8-octanedithiols, $\sim$ 1 nm-thick). A novel method for completing the electrical circuit between the nanoantenna and gold film using an atomic force microscope (AFM) is developed. Based on the results of numerical modeling, the nanoantenna modes exciting the propagating surface plasmon polaritons are identified as hybridized gap and antenna modes. Our results demonstrate the ability to interrogate individual tunneling-driven nanoantennas, a crucial step toward the development of electrical nanosources of surface plasmon polaritons and light.

Keywords

surface plasmon, inelastic electron tunneling, conducting atomic force microscopy, nanoantenna

Introduction

Since the turn of the century, the idea of producing ultrafast and ultracompact circuits and devices using surface plasmon polaritons has propelled an enormous amount of research.[1–5] Surface plasmon polaritons (SPPs) are collective oscillations of electrons on a metal-dielectric interface that are coupled to an electromagnetic wave. Most often, SPPs are excited optically. However, an *electrical*, low energy, integrable nanosource of SPPs is essential if plasmonic circuits are to become a commercial reality. A leading candidate for such an SPP nanosource is a biased tunneling junction.[6]

Metal-insulator-metal (MIM) tunneling junctions have been intensely studied as potential nanosources of surface plasmons[7–10] and light,[11–20] though other material systems[21–23] and geometries[24] have also been considered. The tunneling junction used in this work is shown schematically in Fig. 1 a); two metal electrodes (here a gold nanocube and a thin (50-nm) gold film) are separated by an insulating molecular layer (1,8-octanedithiols, $\sim$ 1 nm-thick). When a potential difference is applied between the two metal electrodes, a tunneling

current may flow. While the vast majority of this current is *elastic*, a small percentage may be *inelastic* and thus able to excite surface plasmon polaritons. The different criteria for optimizing a MIM structure for SPP excitation have been identified;[25–29] the desired SPP mode must be the dominant contribution to the local electromagnetic density of states in the junction so that quenching may be overcome. In order to create such a situation a plasmonic nanoantenna[30] is often used. A nanoantenna can not only improve the efficiency, but also lead to directional emission,[15,31–37] or as is the case here, influence the emission spectrum.[8,9,16,19,20,38]

In this work, we use a gold nanocube both as an antenna and as an electrode to excite propagating surface plasmon polaritons on a gold film with inelastic tunneling electrons. In order to excite propagating surface plasmons on the Au film with this "nanocube-on-a-mirror" tunneling junction, a bias voltage must be applied between the nanocube antenna and the gold film. Here we introduce a new method to locally apply a bias voltage to nanoscale optoelectronic structures using the conducting tip of an atomic force microscope (AFM). Using this approach, several different structures may be tested sequentially on a sample, without the need of lithography-fabricated contact wires for each structure. Note also that using this method, the excitation is restricted to the nanoscale tunneling junction between the antenna and the gold film. This is in contrast to other local electrical excitation techniques leading to the emission of light such as scanning tunneling microscope-induced luminescence[39–47] and cathodoluminescence,[48–51] where the modes of the antenna are primarily excited. Thus this technique opens up new possibilities for the study of electroluminescence at the nanoscale.

Results and discussion

The nanoantenna tunneling junction used to locally and electrically excite surface plasmon polaritons consists of a single-crystalline gold nanocube (typical side lengths 30 to 80 nm) separated from a 50-nm thick gold film on glass by a ~ 1 nm molecular layer (1,8-octanedithiols,

see the *Methods* section for more details and Section S1 of the Supporting Information (SI) for characterization of the Au film with and without the molecular layer). Parts b) and c) of Fig. 1 show a scanning electron and atomic force microscopy image respectively of such a nanocube. A schematic of the experiment and sample is shown in Fig. 1 a) (see also *Methods*). In order to excite SPPs, the metallic (platinum) tip of an atomic force microscope (AFM) electrically contacts the upper face of the nanocube antenna and a voltage difference of 2.5 V is applied between the nanoantenna and Au film. This allows a tunneling current to flow in the nanoscale junction between the antenna and Au layer. The inelastic contribution of this current may excite the different optical modes of the system which have a significant local electromagnetic density of states (LDOS) in the tunneling junction, as would be the case in a future device. This is again in contrast to a technique such as cathodoluminescence where a multitude of modes irrelevant for a device are excited by the high-energy electron beam passing through the entire structure. In our case, the excited modes can then radiate into SPPs propagating on the upper interface of the gold film.[7–9,24] The photons resulting from the leakage of the SPPs through the thin gold film into the glass substrate may then be collected using an oil-immersion objective lens (see the *Methods* section for details).

As a first step, in order to confirm the tunneling nature of the junction and estimate the barrier thickness, an $I(V)$ curve is obtained. In such a measurement, the AFM tip completes the circuit, the applied voltage is ramped and the resulting current is measured. Figure 1 d) shows a typical $I(V)$ characteristic obtained in this way. Such non-linear behaviour is typical of a tunneling junction and may be fit using the model described by Simmons in Ref. [53]. Using the low-voltage approximation for a rectangular barrier ($\alpha = 1$), an average gap thickness of ~ 1.4 nm for the structure and a work function for gold of 1.2 eV are estimated in this example. A junction area of $(70\text{ nm})^2$ is used in the fit since the antenna is considered a cube and a height of 70 nm is measured by AFM in this case. Note that if a similar $I(V)$ measurement is carried out on the gold film, the current saturates the detector immediately. Thus we can conclude that the contact resistance of the AFM tip is negligible compared to

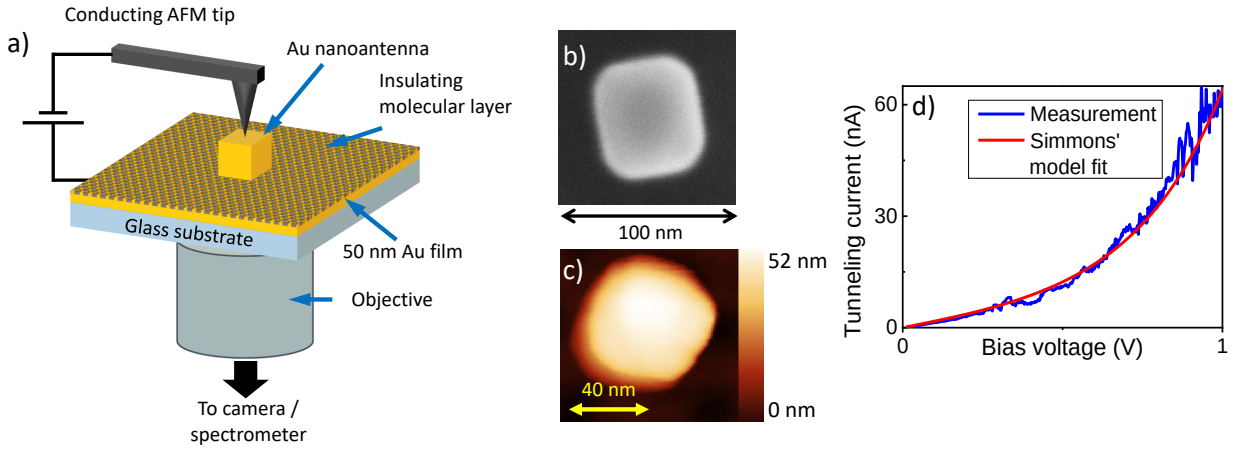

Figure 1: Sample and experiment. The sample consists of a chemically synthesized single-crystalline gold nanocube separated from a 50-nm Au film on glass by a ~ 1 nm insulating layer of 1,8-octanedithiol (C8DT) molecules. a) Schematic of the experiment: a conducting AFM tip is used to locally apply a voltage difference between the gold nanocube antenna and the Au film. The inelastic tunneling current flowing through the tunneling junction formed by the nanocube-insulating layer-gold film "sandwich" excites the optical modes of the system. These modes decay radiatively or non-radiatively and may excite surface plasmon polaritons (SPPs) on the gold film. The photons resulting from the leakage of the SPPs through the thin gold film into the transparent substrate are collected using an oil-immersion objective lens. b) Scanning electron and c) atomic force microscopy (AFM) images of an Au nanocube. Note that for the samples used in the experiments, the nanoparticle density is on the order of 10 particles per 100 μm^2. This low density of nanoantennas is chosen so that the SPPs excited in the experiment are not scattered by neighbouring nanoparticles.[52] d) $I(V)$ curve measured on a "nanocube-on-a-mirror" nanoantenna tunneling junction (blue curve). The voltage difference between the nanoantenna and the gold film is applied via the conducting tip of an atomic force microscope. Using Simmons' model,[53] the shown fit to the data is obtained considering a gap thickness of 1.336 nm, a work function for gold of 1.2 eV and a junction area of (70 nm)^2 (antenna height = 70 nm as measured by AFM). The applied voltage is restricted to $\leq$1 V for technical reasons and so that the Simmons' model remains applicable.[54]

the resistance of the tunneling junction. Once the tunneling nature of the barrier between the antenna and film has been determined, the electrical excitation of SPPs using this junction may be pursued.

Figure 2 shows the result of the experiment when tunneling current flows through the nanoantenna junction and the emitted light below the substrate is detected (2.5 V potential difference applied). Figure 2 a) shows the resulting spatial distribution of the emitted light (real-space image). In this intentionally saturated result, light is seen to be emitted at distances of up to 20 μm from the nanoantenna junction position. This is interpreted as the leakage of SPPs propagating on the upper interface of the Au film into far-field photons in the medium of higher index of refraction (glass).[55,56] The observed spatial distribution of the emitted light is said to reflect that of the SPPs on the upper interface of the Au film.[57,58] The decay of the SPP intensity with propagation is expected due to radiation damping and losses in the metal.[55]

To confirm that the collected light arises from the radiative decay of propagating surface plasmons, an optical Fourier plane image must be acquired under similar conditions (see *Methods*). In Fig. 2 b) the angular distribution of the collected light is measured, or more precisely, the intensity of the collected light as a function of $\frac{k_{||}}{k_0}$, where $k_{||}$ is the component of the wavevector parallel to the substrate and $k_0 = \frac{2\pi}{\lambda_0}$, with λ_0 the free space wavelength. In Fig. 2 b) we observe a thin ring at a value of $\frac{k_{||}}{k_0} = 1.025$, which is expected for SPPs propagating on an air-gold surface with a free-space wavelength of $\sim$ 770 nm.[55,59] This confirms that the collected light is indeed from surface plasmon polaritons that have been excited electrically with the nanoantenna tunneling junction. Further details of the Fourier plane analysis may be found in Section S2 of the Supporting Information.

Figure 3 shows the optical spectrum that is obtained when the nanometer gap between a 40-nm high cubic nanoantenna and a gold film is biased with a potential difference of 2.5 V and the resulting light beneath the substrate is directed towards a spectrometer (see *Methods*). Unlike the single broad feature which is usually seen when the tunneling current

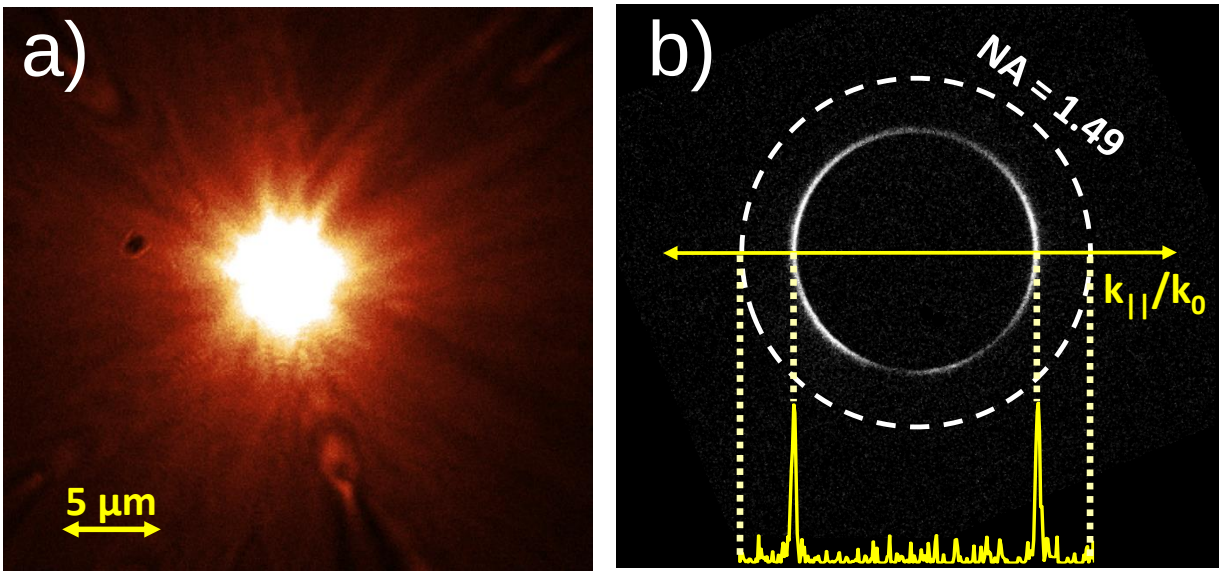

Figure 2: Real and Fourier plane optical microscopy images of the resulting emission when a 2.5 V potential difference is applied between a cubic nanoantenna and a thin gold film that are separated by an insulating molecular layer (the sample is positively biased and the tip is grounded). a) Saturated real plane image showing that light is emitted from a large area ($> (20\ \mu\mathrm{m})^2$), a first indication that the nanoantenna tunneling junction is indeed exciting propagating surface plasmons on the upper interface of the Au film. The irregularities in the image are attributed to imperfections of the surface. b) Fourier plane image showing a ring at the expected $\frac{k_{||}}{k_0}$ value, confirming that surface plasmon polaritons have been excited. As expected for the leakage of SPPs from an air-metal interface into a substrate of higher index of refraction, the plasmon ring is at a value of $\frac{k_{||}}{k_0} > 1$. The measured $\frac{k_{||}}{k_0}$ value is 1.025 ± 0.009, corresponding to the calculated value for SPPs on the air-metal interface of a 50-nm thick gold film on glass at a wavelength of about 770 nm.[55,59] The inset to panel b) is a cross-section obtained along the yellow line. The dashed circle labeled "NA=1.49" represents the numerical aperture of the oil immersion microscope objective used in the measurement. Note that due to the difficulty of the experiments (see *Methods*) the different data sets were obtained using different nanoantenna junctions.

from the non-plasmonic tip of a scanning tunneling microscope (STM) is used to excite SPPs on a thin gold film,[60,61] this spectrum exhibits two distinct peaks. Thus we confirm that the nanoantenna influences the resulting spectrum. In order to understand the origin of these two peaks, simulations are carried out.

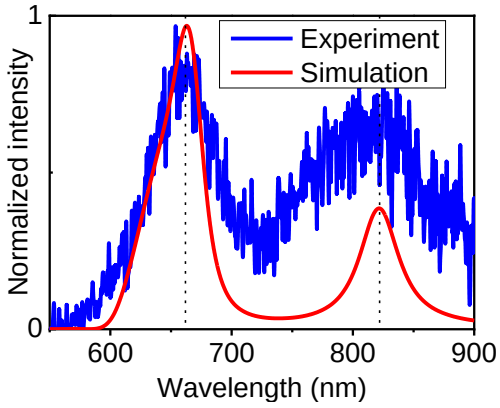

Figure 3: Measured and calculated spectra when a voltage difference of 2.5 V is applied between a 40-nm high cubic nanoantenna and a thin (50-nm) gold film separated by an insulating molecular layer (C8DT). The blue curve is the experimental data, while the red curve is the result from the simulations of Fig. 4. This simulated curve corresponds to the intensity as a function of emission wavelength for an antenna side length of 40 nm, which is the height of the nanoantenna that was measured experimentally. Note that due to the difficulty of the experiments (see *Methods*) the different data sets were obtained using different nanoantenna junctions. For comparison purposes, transmission spectra of a 50-nm gold film with and without the molecular layer may be found in Fig. S2 of the Supporting Information.

To theoretically approximate the inelastic tunneling current in the simulations, a vertical oscillating point dipole source is placed in the center of the gap between the nanoantenna and the gold film.[61,62] The spectrum of this source takes into account the frequency dependence of the probability of an inelastic transition for a given bias voltage (see *Methods* for details).[63] The nanoantenna-film system can support different types of localized optical modes that may be excited by this source: consider first the electric dipole-like localized surface plasmon mode of an isolated nanocube; when such a nanocube approaches a gold film or "mirror" (charge oscillation in the direction perpendicular to the film), this excitation can couple to its image in the film, forming what is known as an antenna mode.[64,65] The lowest order antenna

mode remains electric dipole-like with the fields distributed over the entire structure. A second family of modes that exists in the nanoantenna-on-a-mirror system is the gap or waveguide mode family. These may be thought of as Fabry-Perot-like modes where the electromagnetic energy oscillates horizontally back and forth in the cavity formed by the edges of the nanoantenna[64–68] (i.e., in the direction parallel to the interface). In this case, the fields are strongly enhanced and localized in the gap, with a very small mode volume (on the order of $\frac{\lambda^3}{10^6}$) and a very large local electromagnetic density of states (LDOS).[28] In contrast to these gap modes, the antenna modes have a larger mode volume ($\sim \frac{\lambda^3}{10^4}$) and a smaller LDOS.[28] In addition to this significant difference in mode volume, the gap and antenna modes also differ in their ability to radiate photons and SPPs, with the antenna modes being more radiative than gap modes. These two types of modes may *hybridize* or couple leading to modes which are both "antenna-like" and "gap-like". This hybridization is strongly dependent on the antenna-film distance, which may be easily modified when the separating layer is a molecular film. Varying the molecular layer thickness would be an intuitive way to study the evolution of the resulting hybridized antenna-gap modes.[21]

In order to model this system, an electromagnetic solver based on an aperiodic Fourier modal method dedicated to body-of-revolution structures[69] is used and the nanocube is approximated as a cylinder with an aspect ratio of 1. Details and limitations of the model may be found in the *Methods* section and in Sections S4 and S5 of the Supporting Information respectively. Using this model, the power radiated into the substrate in the collection angle of our optical set-up (NA=1.49) as a function of emission wavelength and antenna side length is calculated. The result is seen in Fig. 4 a). Four clear resonances may be seen in this graph, as denoted by the dashed black and white lines added to guide the eye. Two of these resonances (dashed black lines) are significantly more intense than the others (dashed white lines). The added dashed lines show that the resonance wavelengths vary linearly with antenna side length. As would be expected, the resonances shift to longer wavelength as the antenna size is increased.[28,64]

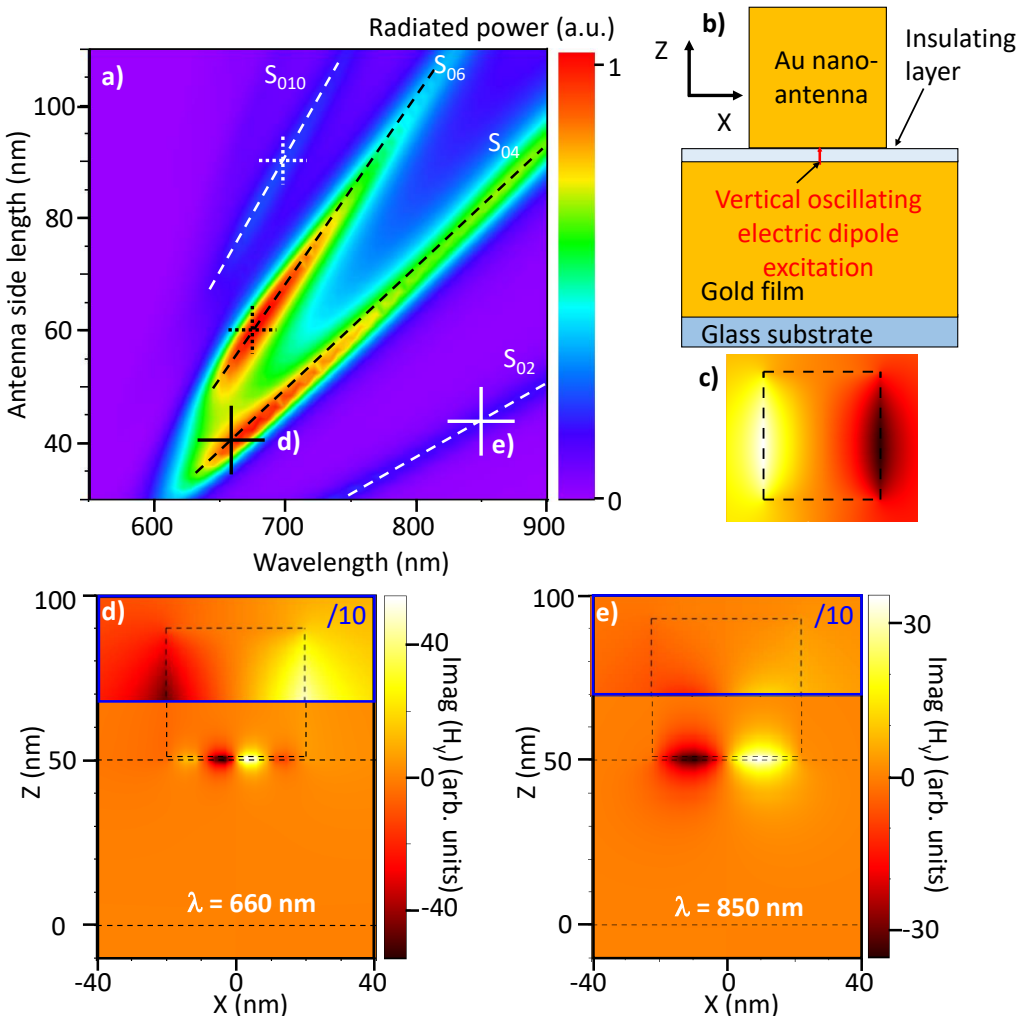

Figure 4: Calculated radiated power as a function of antenna side length and emission wavelength, and mode magnetic field distributions. The cubic antenna is approximated as a cylinder with an aspect ratio of 1. a) The calculated power radiated below the substrate in the collection angle of the objective lens is plotted as a function of antenna side length and wavelength. Several resonances varying linearly with side length may be seen: two faint modes are denoted by white dashed lines while two black dashed lines delineate bright modes. The two continuous crosses mark the wavelengths and antenna side lengths used for the field calculations in parts d) and e) while the field results for the parameters denoted by the dotted crosses may be found in Fig. S5 of the SI. The color scale is linear and in arbitrary units. b) Sketch of the geometry used for the calculation. The thickness of the insulating layer is not to scale. c) Sketch of the magnetic field distribution of an antenna mode. d) and e) Magnetic field distributions in a plane perpendicular to the substrate calculated for the corresponding points marked by continuous crosses in part a). The dashed black lines delineate the antenna and the gold film. An intense field is seen in the region between the antenna and the gold film and is attributed to a gap mode. A lower order mode may be found in part e), at a longer wavelength. The upper parts of the field of view (area enclosed in the blue rectangle) are plotted with a change in colour scale (reduced by a factor of 10). In the upper region of part d) the magnetic field distribution corresponding to an antenna mode is clearly visible; however, no clear evidence of an antenna mode is found when the colour scale is varied in e).

In order to understand the nature of these different resonances and explain the differences in intensities, the field distributions for different antenna side lengths and emission wavelengths are plotted in parts d) and e) of Fig. 4. The particular wavelengths and antenna side lengths considered are denoted by the continuous crosses in part a). The field distributions corresponding to the dotted crosses may be found in Fig. S5 of the Supporting Information. A sketch of a vertical cross-section of the system (i.e., the $X - Z$ plane) is shown in part b); it is in this plane that the fields are calculated. In particular, it is the imaginary part of the y-component of the magnetic field that is shown in parts d) and e). We have chosen to show the magnetic field because the electric-field intensity is dominated by the intense fields around the metal interfaces close to the source. These fields are related to quenching.[70] This contribution prevents a clear identification of the excited modes from the electric-field calculation (see Fig. S6 in the SI). Similarly, i.e., in order to improve the clarity of the figure, the imaginary (and not the real) component of the field is plotted, since there is a singularity in the real component at the source position (singularity in the Green's tensor) which completely saturates the image.

Looking at panels d) and e), we see that the fields are most intense in the gap. The z-component of the electric field (not shown) is also particularly intense in this region; thus the gap modes can couple efficiently to the inelastic tunneling current. A different number of nodes in the magnetic field exists for the different wavelengths shown. Thus from this and other magnetic field calculations for different nanoantenna sizes and wavelengths (see Fig. S5 in the Supporting Information) we can conclude that each resonance corresponds to a different order gap mode, since a different number of nodes in the magnetic field in the gap is found along each dashed line of part a). Using the notation S_{mn} where n is the mode order and m is the azimuthal number (see Section S3 in the Supporting Information), the different gap modes S_{02}, S_{04}, S_{06} and S_{010} are labeled. As would be expected for a Fabry-Perot-like mode, the gap mode resonance wavelength shifts to longer wavelengths as the nanoantenna side length is increased.[16,65]

The upper regions of panels d) and e) in Fig. 4, i.e., the regions delimited by the blue rectangles, have been plotted using a colour scale reduced by a factor of 10. In panel e), the change in colour scale leads to little change in the observations: only a hint of the gap mode may be identified. In panel d), however, the change in colour scale reveals that the magnetic field distribution around the structure is characteristic of the antenna mode discussed in Ref. 28 (see also Fig. S7 in the Supporting Information). Panel c) shows a sketch of the expected magnetic field distribution for such an antenna mode. For such a mode, the field is relatively intense along the sides of the nanoantenna (as opposed to the top or center). Thus we conclude that the two *intense* resonances of panel a) arise from the hybridization (i.e., coupling) of a gap and antenna mode.[28,64,65,68] Indeed, in panel d), the field distributions for both a gap mode as well as for an antenna mode are seen for the same structure at the same wavelength. It has been shown in Ref. 28 that when such gap and antenna modes hybridize, the brightness of the SPP source is increased. Thus, in summary, the "faint" lines seen in the bottom right corner and in the top left section of panel a) correspond to "pure" gap modes, since no evidence of an antenna mode is seen in the field distributions (see the upper regions of panel e) of Fig. 4 and of panel c) of Fig. S5 of the SI). In the case of panel d) in Fig. 4 and panel b) in Fig. S5 in the SI, however, the hybridization with an antenna mode is clear (see the upper regions of the respective figures). The data thus supports the conclusion that the enhancement of the emission seen for antenna side lengths and wavelengths determined from the intense lines in panel a) may be attributed to the coupling between the gap modes and the antenna mode. When the gap and antenna modes couple, we could expect to see an anti-crossing of the modes due to strong coupling. However, due to large mode widths and small coupling strengths (and thus small differences in energy between the hybridized modes), no evidence of strong coupling is observed.[28]

As may also be seen from Fig. 4 a), the spectrum varies with antenna side length; the calculated spectrum of, for example, Fig. 3, is determined from a horizontal cross-section of Fig. 4 a) at the appropriate side length value (40 nm in this case). The spectral variation with

antenna side length is confirmed experimentally (see Fig. S8 in the Supporting Information). The qualitative agreement between the calculations and the experimental results shows that the model captures the essence of the experimental system despite its approximations (see Section S4 in the Supporting Information for further discussion).

Conclusion

In conclusion, using a novel technique based on conducting atomic force microscopy, we have locally and electrically excited surface plasmon polaritons with the inelastic tunneling current in an integrated nanoantenna junction. The nanoantenna has been shown to influence the emission spectrum.Based on the results of numerical modeling, the bright features in the spectrum may be attributed to the emission from hybridized gap and antenna modes.

Optimization of the nanoantenna parameters (aspect ratio, gap thickness and index of refraction) will lead to better antenna performance and other opportunities for controlling the emission (e.g., directionality). Indeed, in the literature it has been shown theoretically that an optimized antenna can achieve an SPP efficiency η_{SPP} of nearly 30% ($\eta_{SPP} = \frac{P_{SPP}}{P_{tot}}$, the ratio of the SPP power to the total power),[28] while for a more sophisticated junction an external quantum efficiency (plasmons/electron) of $\sim 30\%$ and 1 nW of power have been measured experimentally.[24] Thus, with continued optimization and innovation, real-world applications are within reach. Using the conducting AFM tip to complete the circuit and apply a potential difference to the tunneling junction solves the problem of how to easily make a temporary electrical contact at the nanoscale, while nonetheless carrying out sensitive optical measurements. Thus different individual antenna geometries may be tested rapidly on the same sample, without the need for bulky contacts made by lithography. Unlike other local electrical probes such as STM or cathodoluminescence, this new technique is the only approach where the excitation of the plasmonic antenna mode is restricted to the junction between the bottom of the antenna and the film, as it would be in a real device. In the

case of STM excitation of the nanoantenna junction described in this work, two tunneling junctions would exist in series, the second one being the tunneling junction between the STM tip and the top face of the nanoantenna. This second tunneling junction could excite optical modes not accessible to the tunneling junction between the antenna and film.[47,71,72] A similar situation exists in the case of cathodoluminescence.[73–75] Thus our method is the only local electrical probe technique that may be used to test such samples under device-like conditions. This strategy may be easily applied to other situations where nanoscale electrical contacts and optical measurements are necessary, opening up new opportunities for testing optoelectronic circuits on the nanoscale.[76–78]

Methods

Samples: The nanoantennas are single-crystalline gold nanocubes,[79] 30-80 nm in size, synthesized by chemical methods.[80] The insulating molecular layer which forms the tunneling junction between the antenna and gold film consists of 1,8-octanedithiol (C8DT) molecules. The glass substrate is a 170-μm-thick coverslip. A 5-nm Ti adhesion layer is deposited on the glass coverslip before the deposition of the 50-nm-thick gold film by evaporation. A film thickness of 50 nm is chosen as a compromise so as to obtain reasonably long SPP propagation lengths and high enough leakage radiation intensities so that they may be detected. The gold nanocubes are synthesized by adding an Au seed solution to a growth solution, which is then maintained at 30°C until the nanocubes reach the target dimension. The centrifuged Au nanocube solution is then injected into a water-acetonitrile mixture (1:3 v/v) solvent for the partial removal of the CTAB bilayer on the surface of the nanocubes. The CTAB bilayer on the surface of the nanocubes is therefore transformed into a loosely-packed monolayer structure. The "nanoantenna-on-a-mirror" samples are assembled by first immersing the glass substrate with the Au film in an ethanolic 1,8-octanedithiol solution (0.01 M) overnight for surface functionalization. The surface-functionalized Au film is then immersed

in the nanocube solution for $\sim$ 2 h and then gently blown dry with nitrogen. Because the covalent bonding between the Au surface and the thiol group is stronger than the electrostatic interaction between the Au surface and the CTAB molecules, the CTAB molecules on the Au surface in the gap are replaced by 1,8-octanedithiol molecules.[81–83]

This simple alkanedithiolate, 1,8-octanedithiol, was chosen for the insulating layer since the thiol groups on each end bind covalently to gold, and its HOMO-LUMO gap is large, leading to electron tunneling as the main conduction mechanism.[54,84–87] Other possible conduction mechanisms in molecular films include thermionic emission, Poole-Frenkel emission and hopping conduction.[54,84,88] Since the voltage applied in these experiments (2.5 V) is well within the HOMO-LUMO gap of 8-10 eV,[86] the electronic structure of the molecular layer is not expected to affect the inelastic tunneling. Note that the presence of the vibrational modes of the molecules may increase the proportion of inelastic tunneling current, but these modes do not emit light, and the signature of the participation of such modes cannot be observed in $I(V)$ curves at room temperature.[89,90]

AFM / optical microscopy setup: The commercial AFM head is from JPK Instruments (NanoWizard 3). The AFM tips (nominal spring constant 8 N/m) for contacting the nanoantennas are made of platinum and are supplied by Rocky Mountain Nanotechnology. The AFM head is mounted on an inverted optical microscope (Nikon Eclipse Ti-U) which is equipped with an oil immersion objective (Nikon CFI Apochromat 100X 1.49NA TIRF objective). The resulting light from the electrical excitation experiments is collected through the transparent substrate. Real and Fourier plane images are realized by projecting the image or back focal plane on a water-cooled CCD camera (Andor iKon-M) respectively.[91] For the spectral measurements, a real plane image of the sample is projected onto the slit opening of a spectrometer. The reported spectra have been corrected for system response. The imaging spectrometer is from Horiba Jobin Yvon (iHR320 spectrometer with a Synapse CCD detector).

Completing the electrical circuit with the AFM: A voltage is applied to the gold

film using macroscopic clips. Enough pressure is applied (by tightening the appropriate screws) so that the metallic clips pierce the thin molecular layer and form an electrical contact. Good electrical contact is confirmed with a multimeter (whose tip also pierces the molecular layer). In the experiments reported here, the AFM laser diode, used to measure the deflection or amplitude of the AFM cantilever, is a considerable source of background light which masks the signal to be measured. The challenge of the technique is thus to successfully avoid the light from this laser diode while successfully maintaining an electrical contact between the AFM tip and sample. In order to do this, the system is first allowed to thermally stabilize. The conducting AFM tip is then lowered toward the sample until a stable electrical contact is established. The contact resistance is estimated to be ~ 1 kΩ, much less than that of the tunneling junction and thus negligible. During the optical measurement, the laser is shut down while the voltage applied to the piezoelectric element commanding the z-position of the tip is maintained at a constant value, thus maintaining its extension. Note, however, that since the laser is off, there is no feedback keeping the tip-sample interaction constant.

AFM-excitation experiments: In the AFM-excitation experiments, a positive 2.5 V potential is applied to the sample with a 50% duty cycle (period 100 ms) and the tip is grounded. An applied voltage of 2.5 V is chosen so as to excite all the optical modes present in the system at energies below the interband transitions in gold.[92] Such high voltages may be applied to the junction since the area of the junction is small.[9] Since in general shorts are due to defects in the insulating layer, the smaller the junction area, the smaller the defect probability, and the higher the voltage that may be applied. Nonetheless, the non-shorting junction yield is about 10%. The optical signals are integrated for up to a minute, with typical integration times on the order of 20 s. While some junctions shorted almost immediately, others could be used for multiple measurements. The measured current during the optical experiments is typically on the order of μA, but can range from tens of nA to 100 μA.

Simulations: In the simulations, the nanoantenna is approximated as a cylinder with a height and diameter equal to the side length of the nanocube. The molecular film (thickness from $I(V)$ curve) is considered a dielectric with an index of refraction of 1.5 while the refractive index of gold is from Palik.[92] The inelastic tunneling current is represented by a vertical oscillating point dipole positioned in the center of the gap between the cylinder and film. In order to take into account the dependence of the probability of inelastic tunneling on the applied voltage, the simulated spectra are multiplied by the correction factor $1 - \frac{\hbar\omega}{eV_S}$, with V_S the biased voltage applied to the sample (the tip is grounded).[63] Thanks to the symmetry of revolution of the system, the electromagnetic field may be decomposed as a sum of azimuthal eigenmodes where the electromagnetic field for each mode varies as $e^{im\theta}$ with θ the angle in the plane of the film (as usually defined in cylindrical coordinates) and m the azimuthal number. Note that hybridization between two modes is only possible if they have the same azimuthal number.[28] Moreover, only modes with the azimuthal number $m = 0$ may be excited by a vertical point dipole source on the antenna axis. More details on the numerical methods used for this rigorous electromagnetic simulation may be found in Refs. [28, 69].

Acknowledgement

This work was supported by the French National Research Agency (ANR) projects "Intelplan" (ANR-15-CE24-0020) and "ChiC" (ANR-21-CE09-0038). C.Z. acknowledges support from the Safran-IOGS chair on Ultimate Photonics (Ph.D. fellowship).

Supporting Information Available

1. Characterization of the thin Au film with and without the molecular layer
2. Fourier plane analysis

3. Simulation of the emission from a tunneling junction in a "nanoantenna-on-a mirror" geometry

4. Approximations used in the model and additional experimental spectra

5. Dependence of the emission spectrum on the gap thickness

This material is available free of charge via the Internet at http://pubs.acs.org

References

(1) Barnes, W. L.; Dereux, A.; Ebbesen, T. W. Surface plasmon subwavelength optics. *Nature* **2003**, *424*, 824–830.

(2) Atwater, H. A. The promise of plasmonics. *Scientific American* **2007**, *296*, 56–63.

(3) Brongersma, M. L. Introductory lecture: nanoplasmonics. *Faraday Discuss.* **2015**, *178*, 9–36.

(4) Fang, Y. R.; Sun, M. T. Nanoplasmonic waveguides: towards applications in integrated nanophotonic circuits. *Light: Science and Applications* **2015**, *4*, e294.

(5) Davis, T. J.; Gomez, D. E.; Roberts, A. Plasmonic circuits for manipulating optical information. *Nanophotonics* **2017**, *6*, 543–559.

(6) Lambe, J.; McCarthy, S. L. Light Emission from Inelastic Electron Tunneling. *Phys. Rev. Lett* **1976**, *37*, 923–925.

(7) Du, W.; Wang, T.; Chu, H.-S.; Nijhuis, C. A. Highly efficient on-chip direct electronic-plasmonic transducers. *Nature Photonics* **2017**, *11*, 623–627.

(8) Zhang, C.; Hugonin, J.-P.; Coutrot, A.-L.; Sauvan, C.; Marquier, F.; Greffet, J.-J. Antenna surface plasmon emission by inelastic tunneling. *Nature Communications* **2019**, *10*, 4949.

(9) Zhang, C.; Hugonin, J.-P.; Coutrot, A.-L.; Vest, B.; Greffet, J.-J. Electrical generation of visible surface plasmon polaritons by a nanopillars antenna array. *APL Photonics* **2021**, *6*, 056102.

(10) Ochs, M.; Zurak, L.; Krauss, E.; Meier, J.; Emmerling, M.; Kullock, R.; Hecht, B. Nanoscale Electrical Excitation of Distinct Modes in Plasmonic Waveguides. *Nano Letters* **2021**, *21*, 4225–4230.

(11) Kern, J.; Kullock, R.; Prangsma, J.; Emmerling, M.; Kamp, M.; Hecht, B. Electrically Driven Optical Antennas. *Nature Photonics* **2015**, *9*, 582–586.

(12) Parzefall, M.; Bharadwaj, P.; Jain, A.; Taniguchi, T.; Watanabe, K.; Novotny, L. Antenna-coupled photon emission from hexagonal boron nitride tunnel junctions. *Nature Nanotechnology* **2015**, *10*, 1058–1063.

(13) Buret, M.; Uskov, A. V.; Dellinger, J.; Cazier, N.; Mennemanteuil, M.-M.; Berthelot, J.; Smetanin, I. V.; Protsenko, I. E.; Colas-des Francs, G.; Bouhelier, A. Spontaneous Hot-Electron Light Emission from Electron-Fed Optical Antennas. *Nano Lett.* **2015**, *15*, 5811–5818.

(14) Vardi, Y.; Cohen-Hoshen, E.; Shalem, G.; Bar-Joseph, I. Fano Resonance in an Electrically Driven Plasmonic Device. *Nano Letters* **2016**, *16*, 748–752.

(15) Gurunarayanan, S. P.; Verellen, N.; Zharinov, V. S.; James Shirley, F.; Moshchalkov, V. V.; Heyns, M.; Van de Vondel, J.; Radu, I. P.; Van Dorpe, P. Electrically Driven Unidirectional Optical Nanoantennas. *Nano Lett.* **2017**, *17*, 7433–7439.

(16) Qian, H.; Hsu, S.-W.; Gurunatha, K.; Riley, C. T.; Zhao, J.; Lu, D.; Tao, A. R.; Liu, Z. Efficient light generation from enhanced inelastic electron tunnelling. *Nature Photonics* **2018**, *12*, 485–488.

(17) Wang, P.; Krasavin, A. V.; Nasir, M. E.; Dickson, W.; Zayats, A. V. Reactive tunnel junctions in electrically driven plasmonic nanorod metamaterials. *Nature Nanotechnology* **2018**, *13*, 159–164.

(18) Braun, K.; Laible, F.; Hauler, O.; Wang, X.; Pan, A.; Fleischer, M.; Meixner, A. J. Active optical antennas driven by inelastic electron tunneling. *Nanophotonics* **2018**, *7*, 1503–1516.

(19) Qin, J.; Liu, Y.; Luo, H.; Jiang, Z.; Cai, W.; Wang, L. Tunable Light Emission by Electrically Excited Plasmonic Antenna. *ACS Photonics* **2019**, *6*, 2392–2396.

(20) He, X.; Tang, J.; Hu, H.; Shi, J.; Guan, Z.; Zhang, S.; Xu, H. Electrically Driven Highly Tunable Cavity Plasmons. *ACS Photonics* **2019**, *6*, 823–829.

(21) Namgung, S.; Mohr, D. A.; Yoo, D.; Bharadwaj, P.; Koester, S. J.; Oh, S.-H. Ultrasmall Plasmonic Single Nanoparticle Light Source Driven by a Graphene Tunnel Junction. *ACS Nano* **2018**, *12*, 2780–2788.

(22) Parzefall, M.; Szabo, A.; Taniguchi, T.; Watanabe, K.; Luisier, M.; Novotny, L. Light from van der Waals quantum tunneling devices. *Nature Communications* **2019**, *10*, 1–9.

(23) Wang, F.; Liu, Y.; Duffin, T. J.; Kalathingal, V.; Gao, S.; Hu, W.; Guo, Y.; Chua, S.-J.; Nijhuis, C. A. Silicon-Based Quantum Mechanical Tunnel Junction for Plasmon Excitation from Low-Energy Electron Tunneling. *ACS Photonics* **2021**, *8*, 1951–1960.

(24) Qian, H.; Li, S.; Hsu, S.-W.; Chen, C.-F.; Tian, F.; Tao, A. R.; Liu, Z. Highly-efficient electrically-driven localized surface plasmon source enabled by resonant inelastic electron tunneling. *Nature Communications* **2021**, *12*, 3111.

(25) Bigourdan, F.; Hugonin, J.-P.; Marquier, F.; Sauvan, C.; Greffet, J.-J. Nanoantenna

for Electrical Generation of Surface Plasmon Polaritons. *Phys. Rev. Lett.* **2016**, *116*, 106803.

(26) Uskov, A. V.; Khurgin, J. B.; Protsenko, I. E.; Smetanin, I. V.; Bouhelier, A. Excitation of plasmonic nanoantennas by nonresonant and resonant electron tunnelling. *Nanoscale* **2016**, *8*, 14573–14579.

(27) Parzefall, M.; Novotny, L. Light at the End of the Tunnel. *ACS Photonics* **2018**, *5*, 4195–4202.

(28) Zhang, C.; Hugonin, J.-P.; Greffet, J.-J.; Sauvan, C. Surface Plasmon Polaritons Emission with Nanopatch Antennas: Enhancement by Means of Mode Hybridization. *ACS Photonics* **2019**, *6*, 2788–2796.

(29) Parzefall, M.; Novotny, L. Optical antennas driven by quantum tunneling: a key issues review. *Rep. Prog. Phys* **2019**, *82*, 112401.

(30) Novotny, L.; van Hulst, N. Antennas for light. *Nature Photonics* **2011**, *5*, 83–90.

(31) Curto, A. G.; Volpe, G.; Taminiau, T. H.; Kreuzer, M. P.; Quidant, R.; van Hulst, N. F. Unidirectional Emission of a Quantum Dot Coupled to a Nanoantenna. *Science* **2010**, *329*, 930–933.

(32) Kosako, T.; Kadoya, Y.; Hofmann, H. F. Directional control of light by a nano-optical Yagi-Uda antenna. *Nature Photonics* **2010**, *4*, 312–315.

(33) Shegai, T.; Miljkovic, V. D.; Bao, K.; Xu, H. X.; Nordlander, P.; Johansson, P.; Kall, M. Unidirectional Broadband Light Emission from Supported Plasmonic Nanowires. *Nano Letters* **2011**, *11*, 706–711.

(34) Coenen, T.; Vesseur, E. J. R.; Polman, A.; Koenderink, A. F. Directional Emission from Plasmonic Yagi-Uda Antennas Probed by Angle-Resolved Cathodoluminescence Spectroscopy. *Nano Letters* **2011**, *11*, 3779–3784.

(35) Wei, H.; Tian, X.; Pan, D.; Chen, L.; Jia, Z.; Xu, H. Directionally-Controlled Periodic Collimated Beams of Surface Plasmon Polaritons on Metal Film in Ag Nanowire/Al2O3/Ag Film Composite Structure. *Nano Letters* **2015**, *15*, 560–564.

(36) Kullock, R.; Ochs, M.; Grimm, P.; Emmerling, M.; Hecht, B. Electrically-driven Yagi-Uda antennas for light. *Nature Communications* **2020**, *11*, 1–7.

(37) Li, N.; Lai, Y.; Lam, S. H.; Bai, H.; Shao, L.; Wang, J. Directional Control of Light with Nanoantennas. *Advanced Optical Materials* **2021**, *9*, 2001081.

(38) Li, Y.; Hu, H.; Jiang, W.; Shi, J.; Halas, N. J.; Nordlander, P.; Zhang, S.; Xu, H. Duplicating Plasmonic Hotspots by Matched Nanoantenna Pairs for Remote Nanogap Enhanced Spectroscopy. *Nano Letters* **2020**, *20*, 3499–3505.

(39) Gimzewski, J. K.; Sass, J. K.; Schlitter, R. R.; Schott, J. Enhanced Photon-emission In Scanning Tunnelling Microscopy. *Europhysics Letters* **1989**, *8*, 435–440.

(40) Berndt, R.; Gimzewski, J. K.; Johansson, P. Inelastic tunneling excitation of tip-induced plasmon modes on noble-metal surfaces. *Phys. Rev. Lett.* **1991**, *67*, 3796–3799.

(41) Schull, G.; Becker, M.; Berndt, R. Imaging confined electrons with plasmonic light. *Physical Review Letters* **2008**, *101*, 136801.

(42) Dong, Z. C.; Zhang, X. L.; Gao, H. Y.; Luo, Y.; Zhang, C.; Chen, L. G.; Zhang, R.; Tao, X.; Zhang, Y.; Yang, J. L.; Hou, J. G. Generation of molecular hot electroluminescence by resonant nanocavity plasmons. *Nature Photonics* **2010**, *4*, 50–54.

(43) Myrach, P.; Nilius, N.; Freund, H.-J. Photon mapping of individual Ag particles on MgO/Mo(001). *Phys. Rev. B* **2011**, *83*, 035416.

(44) Douillard, L.; Charra, F. High-resolution mapping of plasmonic modes: photoemission and scanning tunnelling luminescence microscopies. *Journal of Physics D-applied Physics* **2011**, *44*, 464002.

(45) Zhang, Y.; Boer-Duchemin, E.; Wang, T.; Rogez, B.; Comtet, G.; Le Moal, E.; Dujardin, G.; Hohenau, A.; Gruber, C.; Krenn, J. R. Edge scattering of surface plasmons excited by scanning tunneling microscopy. *Optics Express* **2013**, *21*, 13938–48.

(46) Kuhnke, K.; Große, C.; Merino, P.; Kern, K. Atomic-Scale Imaging and Spectroscopy of Electroluminescence at Molecular Interfaces. *Chemical Reviews* **2017**, *117*, 5174–5222.

(47) Cao, S.; Zapata-Herrera, M.; Campos, A.; Le Moal, E.; Marguet, S.; Dujardin, G.; Kociak, M.; Aizpurua, J.; Borisov, A. G.; Boer-Duchemin, E. Probing the Radiative Electromagnetic Local Density of States in Nanostructures with a Scanning Tunneling Microscope. *ACS Photonics* **2020**, *7*, 1280–1289.

(48) Gómez-Medina, R.; Yamamoto, N.; Nakano, M.; de Abajo, F. J. G. Mapping plasmons in nanoantennas via cathodoluminescence. *New Journal of Physics* **2008**, *10*, 105009.

(49) Coenen, T.; Bernal Arango, F.; Femius Koenderink, A.; Polman, A. Directional emission from a single plasmonic scatterer. *Nature Communications* **2014**, *5*, 3250.

(50) Kociak, M.; Stéphan, O. Mapping plasmons at the nanometer scale in an electron microscope. *Chem. Soc. Rev.* **2014**, *43*, 3865–3883.

(51) Schmidt, F.-P.; Losquin, A.; Horak, M.; Hohenester, U.; Stöger-Pollach, M.; Krenn, J. R. Fundamental Limit of Plasmonic Cathodoluminescence. *Nano Letters* **2021**, *21*, 590–596.

(52) Wang, T.; Rogez, B.; Comtet, G.; Le Moal, E.; Abidi, W.; Remita, H.; Dujardin, G.; Boer-Duchemin, E. Scattering of electrically excited surface plasmon polaritons by gold nanoparticles studied by optical interferometry with a scanning tunneling microscope. *Phys. Rev. B* **2015**, *92*, 045438.

(53) Simmons, J. G. Generalized Formula for the Electric Tunnel Effect between Similar

Electrodes Separated by a Thin Insulating Film. *Journal of Applied Physics* **1963**, *34*, 1793–1803.

(54) Li, J.-C.; Wang, D.; Ba, D. Effects of Temperature and Light Illumination on the Current-Voltage Characteristics of Molecular Self-Assembled Monolayer Junctions. *The Journal of Physical Chemistry C* **2012**, *116*, 10986.

(55) Raether, H. *Surface Plasmons on Smooth and Rough Surfaces and on Gratings*; Springer Tracts in Modern Physcis; Springer-Verlag, Berlin, 1988; Vol. 111.

(56) Hecht, B.; Bielefeldt, H.; Novotny, L.; Inouye, Y.; Pohl, D. W. Local Excitation, Scattering, and Interference of Surface Plasmons. *Phys. Rev. Lett.* **1996**, *77*, 1889–1892.

(57) Wang, J.; Zhao, C.; Zhang, J. Does the leakage radiation profile mirror the intensity profile of surface plasmon polaritons? *Opt. Lett.* **2010**, *35*, 1944–1946.

(58) Drezet, A.; Genet, C. Imaging Surface Plasmons: From Leaky Waves to Far-Field Radiation. *Phys. Rev. Lett.* **2013**, *110*, 213901.

(59) Burke, J. J.; Stegeman, G. I.; Tamir, T. Surface-polariton-like waves guided by thin, lossy metal films. *Phys. Rev. B* **1986**, *33*, 5186–5201.

(60) Wang, T.; Boer-Duchemin, E.; Zhang, Y.; Comtet, G.; Dujardin, G. Excitation of propagating surface plasmons with a scanning tunnelling microscope. *Nanotechnology* **2011**, *22*, 175201.

(61) Bharadwaj, P.; Bouhelier, A.; Novotny, L. Electrical Excitation of Surface Plasmons. *Phys. Rev. Lett.* **2011**, *106*, 226802.

(62) Johansson, P. Light emission from a scanning tunneling microscope: Fully retarded calculation. *Phys. Rev. B* **1998**, *58*, 10823–10834.

(63) Persson, B. N. J.; Baratoff, A. Theory of photon emission in electron tunneling to metallic particles. *Phys. Rev. Lett.* **1992**, *68*, 3224–3227.

(64) Tserkezis, C.; Esteban, R.; Sigle, D. O.; Mertens, J.; Herrmann, L. O.; Baumberg, J. J.; Aizpurua, J. Hybridization of plasmonic antenna and cavity modes: Extreme optics of nanoparticle-on-mirror nanogaps. *Phys. Rev. A* **2015**, *92*, 053811.

(65) Chikkaraddy, R.; Zheng, X.; Benz, F.; Brooks, L. J.; de Nijs, B.; Carnegie, C.; Kleemann, M.-E.; Mertens, J.; Bowman, R. W.; Vandenbosch, G. A. E.; Moshchalkov, V. V.; Baumberg, J. J. How Ultranarrow Gap Symmetries Control Plasmonic Nanocavity Modes: From Cubes to Spheres in the Nanoparticle-on-Mirror. *ACS Photonics* **2017**, *4*, 469–475.

(66) Yang, J.; Sauvan, C.; Jouanin, A.; Collin, S.; Pelouard, J.-L.; Lalanne, P. Ultrasmall metal-insulator-metal nanoresonators: impact of slow-wave effects on the quality factor. *Opt. Express* **2012**, *20*, 16880–16891.

(67) Lassiter, J. B.; McGuire, F.; Mock, J. J.; Ciracì, C.; Hill, R. T.; Wiley, B. J.; Chilkoti, A.; Smith, D. R. Plasmonic Waveguide Modes of Film-Coupled Metallic Nanocubes. *Nano Letters* **2013**, *13*, 5866–5872.

(68) Baumberg, J. J.; Aizpurua, J.; Mikkelsen, M. H.; Smith, D. R. Extreme nanophotonics from ultrathin metallic gaps. *Nature Materials* **2019**, *18*, 668–678.

(69) Bigourdan, F.; Hugonin, J.-P.; Lalanne, P. Aperiodic-Fourier modal method for analysis of body-of-revolution photonic structures. *J. Opt. Soc. Am. A* **2014**, *31*, 1303–1311.

(70) Yan, W.; Faggiani, R.; Lalanne, P. Rigorous modal analysis of plasmonic nanoresonators. *Phys. Rev. B* **2018**, *97*, 205422.

(71) Le Moal, E.; Marguet, S.; Rogez, B.; Mukherjee, S.; Dos Santos, P.; Boer-Duchemin, E.; Comtet, G.; Dujardin, G. An Electrically Excited Nanoscale Light Source with Active Angular Control of the Emitted Light. *Nano Lett.* **2013**, *13*, 4198–4205.

(72) Lebedev, D. V.; Shkoldin, V. A.; Mozharov, A. M.; Permyakov, D. V.; Dvoretckaia, L. N.; Bogdanov, A. A.; Samusev, A. K.; Golubok, A. O.; Mukhin, I. S. Scanning Tunneling Microscopy-Induced Light Emission and I(V) Study of Optical Near-Field Properties of Single Plasmonic Nanoantennas. *J. Phys. Chem. Lett.* **2021**, *12*, 501.

(73) Garcia de Abajo, F. J.; Kociak, M. Probing the photonic local density of states with electron energy loss spectroscopy. *Phys. Rev. Lett.* **2008**, *100*, 106804.

(74) Garcia de Abajo, F. J. Optical excitations in electron microscopy. *Reviews of Modern Physics* **2010**, *82*, 209–275.

(75) Mohtashami, A.; Coenen, T.; Antoncecchi, A.; Polman, A.; Koenderink, A. F. Nanoscale Excitation Mapping of Plasmonic Patch Antennas. *ACS Photonics* **2014**, *1*, 1134–1143.

(76) Kos, D.; Di Martino, G.; Boehmke, A.; de Nijs, B.; Berta, D.; Földes, T.; Sangtarash, S.; Rosta, E.; Sadeghi, H.; Baumberg, J. J. Optical probes of molecules as nano-mechanical switches. *Nature Communications* **2020**, *11*, 5905.

(77) Kos, D.; Assumpcao, D. R.; Guo, C.; Baumberg, J. J. Quantum Tunneling Induced Optical Rectification and Plasmon-Enhanced Photocurrent in Nanocavity Molecular Junctions. *ACS Nano* **2021**, *15*, 14535–14543.

(78) Cui, X.; Lai, Y.; Ai, R.; Wang, H.; Shao, L.; Chen, H.; Zhang, W.; Wang, J. Anapole States and Toroidal Resonances Realized in Simple Gold Nanoplate-on-Mirror Structures. *Advanced Optical Materials* **2020**, *8*, 2001173.

(79) Chen, Y.; Gu, X.; Nie, C.-G.; Jiang, Z.-Y.; Xie, Z.-X.; Lin, C.-J. Shape controlled growth of gold nanoparticles by a solution synthesis. *Chem. Commun.* **2005**, 4181–4183.

(80) Wu, H.-L.; Kuo, C.-H.; Huang, M. H. Seed-Mediated Synthesis of Gold Nanocrystals with Systematic Shape Evolution from Cubic to Trisoctahedral and Rhombic Dodecahedral Structures. *Langmuir* **2010**, *26*, 12307–12313.

(81) Pramod, P.; Thomas, K. G. Plasmon Coupling in Dimers of Au Nanorods. *Advanced Materials* **2008**, *20*, 4300–4305.

(82) Cui, X.; Qin, F.; Lai, Y.; Wang, H.; Shao, L.; Chen, H.; Wang, J.; Lin, H.-q. Molecular Tunnel Junction-Controlled High-Order Charge Transfer Plasmon and Fano Resonances. *ACS Nano* **2018**, *12*, 12541–12550.

(83) Cui, X.; Lai, Y.; Qin, F.; Shao, L.; Wang, J.; Lin, H.-Q. Strengthening Fano resonance on gold nanoplates with gold nanospheres. *Nanoscale* **2020**, *12*, 1975–1984.

(84) Wang, W.; Lee, T.; Reed, M. A. Mechanism of electron conduction in self-assembled alkanethiol monolayer devices. *Phys. Rev. B* **2003**, *68*, 035416.

(85) Xu, B. Modulating the conductance of a Au-octanedithiol-Au molecular junction. *Small* **2007**, *3*, 2061–2065.

(86) Akkerman, H. B.; Naber, R. C. G.; Jongbloed, B.; van Hal, P. A.; Blom, P. W. M.; de Leeuw, D. M.; de Boer, B. Electron tunneling through alkanedithiol self-assembled monolayers in large-area molecular junctions. *Proceedings of the National Academy of Sciences of the United States of America* **2007**, *104*, 11161–11166.

(87) Kim, C. M.; Bechhoefer, J. Conductive probe AFM study of Pt-thiol and Au-thiol contacts in metal-molecule-metal systems. *J. Chem. Phys.* **2013**, *138*, 014707.

(88) Aswal, D.; Lenfant, S.; Guerin, D.; Yakhmi, J.; Vuillaume, D. Self assembled monolayers on silicon for molecular electronics. *Anal. Chim. Acta* **2006**, *568*, 84–108.

(89) Wang, W.; Lee, T.; Reed, M. A. Electron tunnelling in self-assembled monolayers. *Reports on Progress in Physics* **2005**, *68*, 523.

(90) Song, H.; Kim, Y.; Jang, Y. H.; Jeong, H.; Reed, M. A.; Lee, T. Observation of molecular orbital gating. *Nature* **2009**, *462*, 1039–1043.

(91) Cao, S.; Le Moal, E.; Bigourdan, F.; Hugonin, J.-P.; Greffet, J.-J.; Drezet, A.; Huant, S.; Dujardin, G.; Boer-Duchemin, E. Revealing the spectral response of a plasmonic lens using low-energy electrons. *Phys. Rev. B* **2017**, *96*, 115419.

(92) Palik, E. D., Ed. *Handbook of optical constants of solids III*; Academic Press: New York, 1998.

TOC Graphic

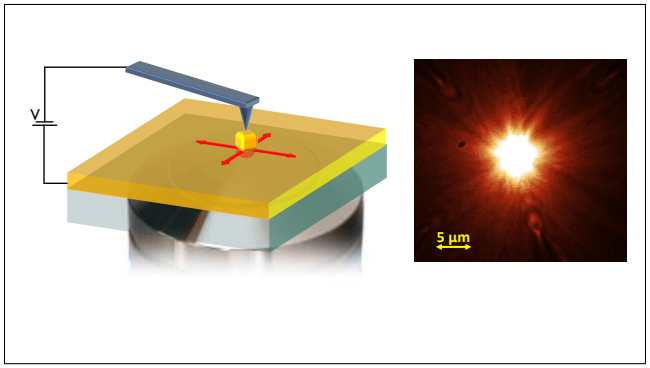

For Table of Contents Use Only

Article title: **Nanoscale electrical excitation of surface plasmon polaritons with a nanoantenna tunneling junction**.

Authors: Delphine Pommier, Zélie Hufschmitt, Cheng Zhang, Yunhe Lai, Gérald Dujardin, Eric Le Moal, Christophe Sauvan, Jean-Jacques Greffet, Jianfang Wang, and Elizabeth Boer-Duchemin

Description of TOC entry: (left image): In this work, a nanoantenna tunneling junction is used to electrically excite surface plasmon polaritons (SPPs) on the nanoscale. A single-crystal, cubic nanoantenna is separated from a thin (50-nm) gold film by a ~ 1 nm-thick insulating molecular layer, thus forming a metal-insulator-metal tunneling junction. To bias this tunneling junction, a new method using the conducting tip of an atomic force microscope to locally and temporarily complete the electrical circuit is developed. When a potential difference is applied between the cubic gold nanoantenna and the Au film, the inelastic component of the tunneling current excites propagating surface plasmons. (right image): These SPPs decay into photons in the glass substrate and are collected using an oil immersion objective to form the real plane image shown here. From this image we see that light is emitted far (several microns) from the excitation position in the center, suggesting that indeed, *propagating* surface plasmons have been excited.